



Cite this: *Chem. Commun.*, 2021, **57**, 1368

Received 7th October 2020,
 Accepted 4th January 2021

DOI: 10.1039/d0cc06693a

rsc.li/chemcomm

Sulfurization-induced partially amorphous palladium sulfide nanosheets for highly efficient electrochemical hydrogen evolution†

Yihui Wang,^a Kai Xu,^a Zizheng Zhu,^a Wen Guo,^a Tingting Yu,^a Maoshuai He,^b Wenxian Wei^{*c} and Tao Yang  ^{*a}

A partially amorphous palladium sulfide was synthesized by sulfurizing crystalline palladium nanosheets facilely, which shows excellent activity and stability towards hydrogen evolution in alkaline media, even superior to the performance of the commercial Pt/C catalyst. The enhanced performance could be attributed to the amorphization transformation and the nanosheet morphology.

Exploiting sustainable energy sources must be one of the most critical issues for global development for quite a long time in the future.¹ Due to the high gravimetric energy density, hydrogen has been considered as one of the most promising energy carriers, which should be produced cleanly and sustainably.^{2–5} Electrochemical water splitting stands out as a competitive way to produce high-purity hydrogen with carbon-free emissions from abundant water.^{6–8} The hydrogen evolution reaction (HER) at a cathode requires highly efficient electro-catalysts to achieve low-temperature operation at small overpotential.^{9–11} Compared with an acid environment, alkaline media display many superiorities, such as a less corrosive environment, weaker ion-adsorption, and faster kinetics.^{12–15} Thus, exploring highly efficient electro-catalyst materials used in an alkaline environment is attracting more and more research interest.^{16–19}

Recently, numerous research studies have been focused on transition metal sulfides (TMSs), such as CoS₂,^{17,18} Ni₃S₂,^{20,21} NiCoS,²² MoS₂,^{23–25} and Rh₂S₃,²⁶ which display suitable d-band positions and active sites for the HER.^{27,28} In particular, amorphous materials have shown better activity than their crystalline counterparts due to the more exposed active sites.^{29–35} For example, for the current density of 10 mA cm⁻², amorphous MoS_x films showed an

overpotential (η_{10}) of 200 mV,³⁶ amorphous Ni-Co complexes exhibited a η_{10} of 70 mV,³⁷ and amorphous Co-doped MoS₂ displayed a η_{10} of 110.5 mV.³⁰ Amorphous NiO achieved 5 mA cm⁻² at an overpotential of 110 mV.³⁸ Nevertheless, the HER activity of these TMSs still falls far short of expectations.¹⁶

Palladium sulfide is an emerging catalyst, displaying excellent activities in acetylene hydrogenation,³⁹ electrochemical oxygen reduction and methanol oxidization,^{40,41} photocatalytic hydrogen generation,⁴² photochemical degradation of herbicides,⁴³ etc. However, the catalytic activity towards the HER has rarely been reported.⁴⁴ Encouraged by the aforementioned advance in PdS and amorphous materials, amorphization of palladium sulfides could be possible to enhance the activity towards the HER. Herein we report an improved HER activity on a partially amorphous palladium sulfide (PAPS) surface in alkaline solution. The partial amorphization was achieved by sulfurizing crystalline Pd nanosheets facilely. Compared with the η_{10} for the current density of 10 mA cm⁻² on crystal PdS planes (198 mV), the present PAPS displayed a little η_{10} of 49 mV. After a durability test of 10 000 cycles LSV, the η_{10} is 65 mV, still smaller than that of most reported HER catalysts.

The PdS nanosheets were synthesized through a two-step process. Crystalline Pd nanosheets were firstly prepared by reducing Pd(acac)₂ under an oxygen-free environment with carbon monoxide at 210 °C. The PdS nanosheets were then produced by reacting Pd nanosheets with sulfur in the same solution. Transmission electron microscopy (TEM) images in Fig. 1A and Fig. S1 (ESI†) show that the Pd products have dominant sheet-like morphology. The difference in contrast indicates that the nanosheets are composed of a thin center and thick edges. Fig. 2B is the corresponding selected area electronic diffraction (SAED) pattern, in which the bright spots suggest the highly crystalline nature of the nanosheets. The concentric rings can be tentatively attributed to the (111), (200), (220) and (311) planes of the fcc Pd. Fig. 1C shows the high-resolution TEM (HRTEM) image of the nanosheets. The distinct lattice spacing of 2.25 Å should be assigned to the (111) planes

^a School of Environmental and Chemical Engineering, Jiangsu Ocean University, Lianyungang 222005, Jiangsu, China. E-mail: yangtao_hit@163.com

^b State Key Laboratory of Eco-Chemical Engineering, Ministry of Education, College of Chemistry and Molecular Engineering, Qingdao University of Science and Technology, Qingdao 266042, Shandong, China

^c Testing Center, Yangzhou University, Yangzhou 225009, Jiangsu, China

† Electronic supplementary information (ESI) available. See DOI: 10.1039/d0cc06693a

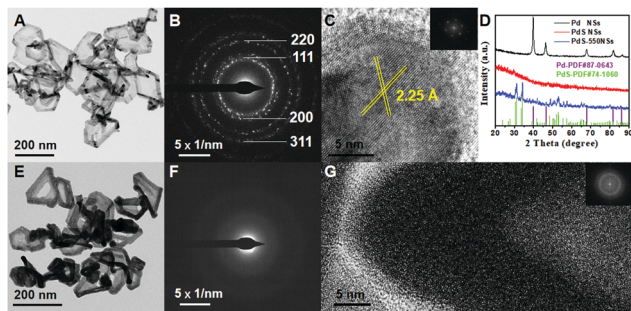


Fig. 1 (A) TEM image of the Pd nanosheets, (B) the corresponding SAED pattern, (C) HRTEM of the Pd nanosheets (inset is the corresponding FFT pattern), (D) XRD patterns of the Pd nanosheets, PdS nanosheets and PdS-550, (E) TEM image of the PdS nanosheets, (F) the corresponding SAED pattern, and (G) HRTEM image of the PdS nanosheets (the inset is the corresponding FFT pattern).

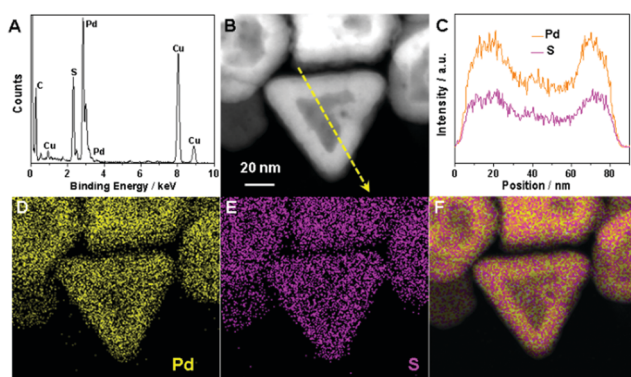


Fig. 2 (A) EDX spectrum of the partially amorphous product, (B) HAADF-STEM image, (C) EDX cross-sectional compositional line scanning and (D–F) EDX elemental mapping images of Pd, S and their merged image.

of Pd. The corresponding FFT pattern suggests the single crystalline feature (inset of Fig. 1C). The XRD pattern in Fig. 1D shows that the nanosheets are fcc structured crystalline Pd, highly in agreement with the SAED results. Fig. 1E and Fig. S2 (ESI[†]) are the TEM images of the sulfurized product; the outlines and the thick edges are still preserved, while some of the center portions have been destroyed. The TEM-EDX spectrum shows that the partially amorphous products are composed of Pd and S with an atomic ratio of 2:3 (Fig. S3, ESI[†]). It is interesting that all of the diffraction peaks in the sulfurized sample weakened to a negligible extent, indicating that the crystalline structure has nearly converted into amorphous structure (Fig. 1D). Correspondingly, the SAED pattern in Fig. 1F shows no diffraction spots. No lattice fringes can be observed in the HRTEM image (Fig. 1G). It has been reported that the interaction between Pd and sulfide is very strong and the lattice constant of PdS is much larger than that of pristine Pd. As a result, lattice expansion would occur fast at such high temperature to accommodate the lattice discrepancy, which will destroy the regular arrangement of Pd atoms and transform the crystalline phase into a partially amorphous structure.⁴⁵ After a post-treatment at 550 °C, the partially amorphous structure transformed to a

crystalline phase, highly in agreement with that of the standard PdS XRD pattern (Fig. 1D). The HRTEM image shows the distinct lattice fringes of PdS of the (130) and (220) planes (Fig. S4, ESI[†]). Elemental mapping shows that Pd and S are still highly distributed in the PdS NSs (Fig. S5, ESI[†]). Therefore, all of the above results clearly indicate the amorphization transformation during sulfurizing crystalline Pd NSs into PdS NSs. For comparison, crystalline PdS nanoparticles with an atomic ratio of 4:1 in the range of 10–15 nm were synthesized (Fig. S6–S8, ESI[†]).

To further understand the chemical composition of the compound, TEM-EDX and elemental mapping were then performed. Fig. 2A shows that the partially amorphous product is composed of Pd and S. A high angle annular dark field (HAADF) scanning TEM (STEM) image is presented in Fig. 2B, the thicker edges and the thinner center portion can be clearly observed. The difference in thickness and the elemental distribution are also reflected through the EDX cross-sectional compositional line scanning (Fig. 2C). Corresponding with the HAADF-STEM image, the edge regions show higher elemental signal intensity than that of the center region. The elemental distribution was further demonstrated through EDX elemental scanning (Fig. 2D–F). The element distribution of Pd and S is highly conformed with the nanosheet profile and the spot densities are highly corresponding to the brightness variation in the HAADF-STEM images. These results in the EDX scan indicate that the partially amorphous product is composed of Pd and S with highly uniform distributions.

Fig. 3 presents the X-ray photoelectron spectroscopy (XPS) spectra of Pd and S for Pd NSs, PdS-550 NSs and Pd₄S NPs. Two pairs of Pd 3d peaks with the binding energies between 343–338 eV and 337–333 eV match the Pd 3d_{3/2} and 3d_{5/2}, respectively. In the XPS spectra of S 2p, the shoulder peaks close to 162 eV should be ascribed to S²⁻ and S₂²⁻. After the treatment at 550 °C, a peak at ~168 eV for the formation of sulfur oxide species appears due to the oxidization of S. Much larger peaks for sulfur oxide species were observed on the PdS NPs. The atomic ratio of Pd and S calculated from the XPS spectra is nearly 1:1. Considering the XPS and TEM-EDX results together, the content of S in the nearly surface regions is slightly higher than the inner structure.

PdS has been investigated as a catalyst for various chemical reactions, such as hydrogenation,³⁹ photo-electrochemical

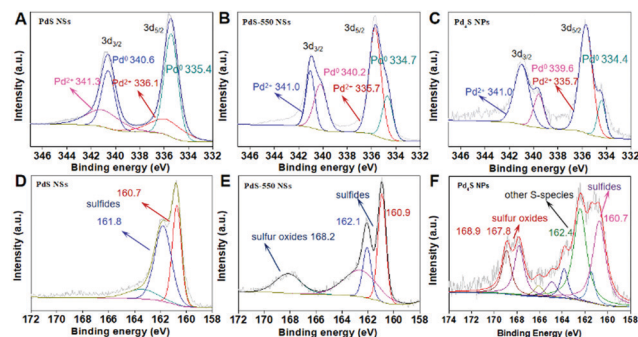


Fig. 3 XPS spectra of Pd for (A) Pd NSs, (B) PdS-550 NSs and (C) Pd₄S NPs. XPS spectra of S for (D) Pd NSs, (E) PdS-550 NSs and (F) Pd₄S NPs.

hydrogen evolution,⁴² oxygen reduction,⁴¹ methanol oxygen,⁴⁰ and photocatalytic degradation of organics.⁴³ However, the electrochemical hydrogen evolution from water on PdS has rarely been reported. Herein, to explore the application of palladium sulfides as HER electrocatalysts in an alkaline environment, the crystalline Pd NSs, partially amorphous PdS NSs, crystalline PdS-550 NSs and the normal PdS NPs were all loaded onto the carbon support before HER measurements. The electrochemical HER activities of these catalysts were investigated in a typical three-electrode system by using a rotating disk electrode (RDE) in Ar saturated 1.0 M KOH solution at a scanning rate of 10 mV s⁻¹. For comparison, commercial Pt/C (20 wt%) and Pd/C (10 wt%) were also tested under the same conditions. The HER polarization curves of PdS NSs, Pt/C, Pd NSs, Pd/C, PdS-550 NSs and PdS NPs are shown in Fig. 4A. The commercial Pd/C and the normal PdS NPs showed the lowest activities, even inferior to that of the Pd NSs. The commercial Pt/C displayed an activity similar to the previous literature reports. Most interesting, the partially amorphous PdS NSs achieved a higher activity than the commercial Pt/C. After a post-treatment at 550 °C, the activity of the crystalline PdS NSs decreased heavily. Clearly, as shown, the alkaline HER activity of the PdS-550 NSs is much lower than those of PdS NSs, demonstrating the essential role of the confined disordered arrangement of atoms in enhancing the HER activities.

To achieve a typical current density of 10 mA cm⁻² (Fig. 4B), the critical value for solar fuel conversion devices, partially amorphous PdS NSs require a small overpotential of 49 mV, much lower than those of crystalline PdS-550 NSs (198 mV) and normal PdS NPs (337 mV), and even superior to that of Pt/C (55 mV). As far as we know, this is the best activity in metal sulfides towards the HER in alkaline media (Table S1, ESI[†]). In addition, the HER current densities on the partially amorphous PdS NSs increased very sharply in the high overpotential region, suggesting a low resistance. Impressively, to obtain the large

HER current density of 50 mA cm⁻², the overpotential of the partially amorphous PdS NSs is 150 mV. In comparison, commercial Pt/C needs 192 mV for the counterpart current density. Even at much higher current density of 100 mA cm⁻², the overpotential on the partially amorphous PdS NSs is only 233 mV. The performance at large current densities suggests quite promising practical applications in industry.

The Tafel slope of partially amorphous PdS NSs is in the range of Volmer (118.2 mV dec⁻¹) and Heyrovsky (39.4 mV dec⁻¹) (Fig. S9, ESI[†]), suggesting a Volmer–Heyrovsky mechanism ((H₂O + e⁻ = H_{ads} + OH⁻ and H₂O + e⁻ + H_{ads} = H₂ + OH⁻). Partially amorphous PdS NSs also show slightly larger double-layer capacitance than those of crystalline Pd-550 NSs and PdS NPs, indicating a larger electrochemical active surface area (EASA) (Fig. S10, ESI[†]). Stability was then evaluated through a 10 000 times successive LSV scanning of the HER. The polarization curves for the HER were recorded intermittently (Fig. 4C). After the first drop after 500 times LSV, the activity decreased very slowly and the overpotential for 10 mA cm⁻² only dropped 16 mV after 10 000 times LSV scans. A time-dependent current density curve was also performed at an overpotential of 49 mV (Fig. S11, ESI[†]). The current density for the HER was above 10 mA cm⁻² in 29 400 s and dropped to 9.1 mA cm⁻² at the final 30 000 s. Electrochemical impedance spectroscopy (EIS) was performed on the three sulfides at open-circuit voltage (Fig. 4D). Partially amorphous PdS NS shows the smallest resistance for the HER, allowing a better performance (Fig. S12, ESI[†]). The small resistance in the partially amorphous structure has been observed in other amorphous systems.³⁸

In summary, we have demonstrated a promising partially amorphous PdS electrocatalyst for hydrogen evolution, which can be synthesized through sulfurizing crystalline Pd nanosheets. Electrochemical measurements reveal that the as-obtained partially amorphous PdS nanosheets displayed ultrahigh catalytic performance towards the HER, higher than that of the crystalline PdS, and even superior to that of the commercial Pt/C catalyst. The excellent performance should be mainly due to the partial amorphization of PdS and the nanosheet morphology.

This work was financially supported by the National Natural Science Foundations of China (NSFC) (No. 21473067), Six Talent Peaks Project of Jiangsu Province (XCL-004), the Key Project of “HaiYan” Program of Lianyungang (No. 2017-ZD-004), the Natural Science Foundation of Jiangsu Province (No. BK20201466 and BK20181074), the Graduate Research Innovation Program of Jiangsu Province (No. KYCX19_2258, KYCX20_2921, KYCX20_2919), the Key University Science Research Project of Jiangsu Province (No. 19KJA430007), and the project funded by the Priority Academic Program Development of Jiangsu Higher Education Institutions (PAPD).

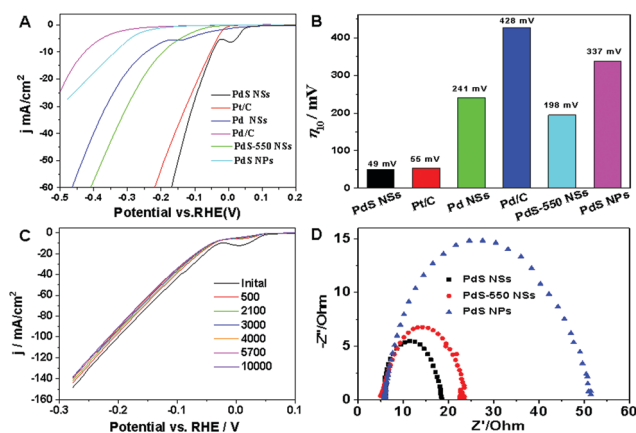


Fig. 4 Catalytic performance of PdS NSs. (A) The polarization curves and (B) overpotential for 10 mA cm⁻² of PdS NSs compared with Pd NSs, PdS-550 NSs, PdS NPs, commercial Pt/C, and commercial Pd/C. (C) Durability test of PdS NSs for the HER. (D) EIS spectra of PdS NSs, PdS-550 NSs and PdS NPs.

Conflicts of interest

There are no conflicts to declare.

Notes and references

- J. Kibsgaard, T. F. Jaramillo and F. Besenbacher, *Nat. Chem.*, 2014, **6**, 248–253.
- Q. Yun, Q. Lu, X. Zhang, C. Tan and H. Zhang, *Angew. Chem., Int. Ed.*, 2018, **57**, 626–646.
- B. Y. Xiong, L. S. Chen and J. L. Shi, *ACS Catal.*, 2018, **8**, 3688–3707.
- J.-Y. Zhang, H. Wang, Y. Tian, Y. Yan, Q. Xue, T. He, H. Liu, C. Wang, Y. Chen and B. Y. Xia, *Angew. Chem., Int. Ed.*, 2018, **57**, 7649–7653.
- S. Sarkar and S. C. Peter, *Inorg. Chem. Front.*, 2018, **5**, 2060–2080.
- Y. Zheng, Y. Jiao, M. Jaroniec and S. Z. Qiao, *Angew. Chem., Int. Ed.*, 2015, **54**, 52–65.
- Y. Ding, B.-Q. Miao, Y.-C. Jiang, H.-C. Yao, X.-F. Li and Y. Chen, *J. Mater. Chem. A*, 2019, **7**, 13770–13776.
- H. Huang, Y. Zhao, Y. Bai, F. Li, Y. Zhang and Y. Chen, *Adv. Sci.*, 2020, **7**, 2000012.
- P. Alexa, J. M. Lombardi, P. Abufager, H. F. Busnengo, D. Grumelli, V. S. Vyas, F. Haase, B. V. Lotsch, R. Gutzler and K. Kern, *Angew. Chem., Int. Ed.*, 2020, **59**, 8411–8415.
- H. Chen, X. Ai, W. Liu, Z. Xie, W. Feng, W. Chen and X. Zou, *Angew. Chem., Int. Ed.*, 2019, **58**, 11409–11413.
- L. Chen, L.-R. Zhang, L.-Y. Yao, Y.-H. Fang, L. He, G.-F. Wei and Z.-P. Liu, *Energy Environ. Sci.*, 2019, **12**, 3099–3105.
- X. Ge, A. Sumboja, D. Wu, T. An, B. Li, F. W. T. Goh, T. S. A. Hor, Y. Zong and Z. Liu, *ACS Catal.*, 2015, **5**, 4643–4667.
- M. Liu, R. Zhang and W. Chen, *Chem. Rev.*, 2014, **114**, 5117–5160.
- M. K. Debe, *Nature*, 2012, **486**, 43–51.
- W. Wang, Y. Zhao and Y. Ding, *Nanoscale*, 2015, **7**, 11934–11939.
- C. Hu, L. Zhang and J. Gong, *Energy Environ. Sci.*, 2019, **12**, 2620–2645.
- X. Zeng, M. J. Jang, S. M. Choi, H.-S. Cho, C.-H. Kim, N. V. Myung and Y. Yin, *Mater. Chem. Front.*, 2020, **4**, 2307–2313.
- X. Zeng, Y. Bai, S. M. Choi, L. Tong, R. M. Aleisa, Z. Li, X. Liu, R. Yu, N. V. Myung and Y. Yin, *Mater. Today Nano*, 2019, **6**, 100038.
- J.-Q. Chi, X.-J. Zeng, X. Shang, B. Dong, Y.-M. Chai, C.-G. Liu, M. Marin and Y. Yin, *Adv. Funct. Mater.*, 2019, **29**, 1901790.
- G. Li, X. Cui, B. Song, H. Ouyang, K. Wang, Y. Sun and Y. Wang, *Chem. Eng. J.*, 2020, 388.
- S. Huang, Y. Meng, Y. Cao, F. Yao, Z. He, X. Wang, H. Pan and M. Wu, *Appl. Catal., B*, 2020, 274.
- A. Irshad and N. Munichandraiah, *ACS Appl. Mater. Interfaces*, 2017, **9**, 19746–19755.
- C. Meng, X. Chen, Y. Gao, Q. Zhao, D. Kong, M. Lin, X. Chen, Y. Li and Y. Zhou, *Molecules*, 2020, 25.
- J. Jian, Y. Li, H. Bi, X. Wang, X. Wu and W. Qin, *ACS Sustainable Chem. Eng.*, 2020, **8**, 4547–4554.
- X. Ding, T. Yang, W. Wei, Y. Wang, K. Xu, Z. Zhu, H. Zhao, T. Yu and D. Zhang, *Catal. Sci. Technol.*, 2020, **10**, 3247–3254.
- D. Yoon, B. Seo, J. Lee, K. S. Nam, B. Kim, S. Park, H. Baik, S. H. Joo and K. Lee, *Energy Environ. Sci.*, 2016, **9**, 850–856.
- K. Liang, S. Pakhira, Z. Yang, A. Nijamudheen, L. Ju, M. Wang, C. I. Aguirre-Velez, G. E. Sterbinsky, Y. Du, Z. Feng, J. L. Mendoza-Cortes and Y. Yang, *ACS Catal.*, 2018, **9**, 651–659.
- B. Seo and S. H. Joo, *Nano Convergence*, 2017, **4**, 19.
- H. Zhao, X. Chen, G. Wang, Y. Qiu and L. Guo, *2D Mater.*, 2019, **6**, DOI: 10.1088/2053-1583/ab1169.
- H. Zhang, Y. Li, T. Xu, J. Wang, Z. Huo, P. Wan and X. Sun, *J. Mater. Chem. A*, 2015, **3**, 15020–15023.
- H. Vrubel, T. Moehl, M. Grätzel and X. Hu, *Chem. Commun.*, 2013, **49**, 8985–8987.
- M. L. Tang, D. C. Grauer, B. Lassalle-Kaiser, V. K. Yachandra, L. Amirav, J. R. Long, J. Yano and A. P. Alivisatos, *Angew. Chem.*, 2011, **123**, 10385–10389.
- C. G. Morales-Guio and X. Hu, *Acc. Chem. Res.*, 2014, **47**, 2671–2681.
- G. Wu, X. Zheng, P. Cui, H. Jiang, X. Wang, Y. Qu, W. Chen, Y. Lin, H. Li, X. Han, Y. Hu, P. Liu, Q. Zhang, J. Ge, Y. Yao, R. Sun, Y. Wu, L. Gu, X. Hong and Y. Li, *Nat. Commun.*, 2019, **10**, 4855.
- Y. Chen, Z. Lai, X. Zhang, Z. Fan, Q. He, C. Tan and H. Zhang, *Nat. Rev. Chem.*, 2020, **4**, 243–256.
- J. D. Benck, Z. Chen, L. Y. Kuritzky, A. J. Forman and T. F. Jaramillo, *ACS Catal.*, 2012, **2**, 1916–1923.
- H. Li, S. Chen, X. Jia, B. Xu, H. Lin, H. Yang, L. Song and X. Wang, *Nat. Commun.*, 2017, **8**, 15377.
- X. Yan, L. Tian and X. Chen, *J. Power Sources*, 2015, **300**, 336–343.
- Y. Liu, A. J. McCue, J. Feng, S. Guan, D. Li and J. A. Anderson, *J. Catal.*, 2018, **364**, 204–215.
- R. Nandan and K. K. Nanda, *Nanoscale*, 2017, **9**, 12628–12636.
- C. Du, P. Li, F. Yang, G. Cheng, S. Chen and W. Luo, *ACS Appl. Mater. Interfaces*, 2018, **10**, 753–761.
- M. Barawi, I. J. Ferrer, J. R. Ares and C. Sánchez, *ACS Appl. Mater. Interfaces*, 2014, **6**, 20544–20549.
- L.-L. Long, A.-Y. Zhang, Y.-X. Huang, X. Zhang and H.-Q. Yu, *J. Mater. Chem. A*, 2015, **3**, 4301–4306.
- Y. Wen, H. Zhu, L. Zhang, J. Hao, C. Wang, S. Zhang, S. Lu, M. Zhang and M. Du, *ACS Appl. Energy Mater.*, 2019, **2**, 2013–2021.
- H. Cheng, N. Yang, G. Liu, Y. Ge, J. Huang, Q. Yun, Y. Du, C. J. Sun, B. Chen, J. Liu and H. Zhang, *Adv. Mater.*, 2020, **32**, e1902964.